EVS30 Symposium
Stuttgart, Germany, October 9 - 11, 2017

The Effect of Inerter and Relaxation Spring on Passive Suspensions of Electric Vehicles with In-wheel Motors

Liunan Yang[1], Kesavan Ramakrishnan, Federico Ballo, Giorgio Previati, Massimiliano Gobbi, Gianpiero Mastinu

[1]*Liunan Yang (corresponding author), Politecnico di Milano. Milan, 20158, Italy. liunan.yang@polimi.it*

Abstract

The increased unsprung mass caused by the in-wheel motor influences the ride performance of the vehicle. In order to reduce the impact, passive suspension components such as inerter and relaxation spring can be introduced. A linear quarter-car model is used to represent the vehicle corner. The suspension architectures featuring inerter and/or relaxation spring are compared with conventional passive suspension by considering three performance indices. The suspension performance indices, namely, discomfort index, road holding index, and working space index are derived analytically. It is proven that the suspension architectures with inerter and/or relaxation spring provide improved performance when they are arranged in specific layouts.

Keywords: wheel hub motor, EV (electric vehicle), vehicle performance, modeling.

1 Introduction

An electric vehicle powertrain with in-wheel motors offers improved efficiency and compact packing layout. A wide variety of solutions such as Michelin Active Wheel, e-Traction TheWheel, and Protean Drive [1, 2, 3, 4] are available on the market for both passenger cars and commercial vehicles. However, the shortcomings due to the increased unsprung mass are non-negligible [5]. Based on the sensitivity analysis presented in [6], the increase of unsprung mass has a negative influence on the suspension dynamic behaviour.

Recent studies including the lightweight design of in-wheel motors [7], isolation of motor vibration [8], and active suspension [9] have evaluated the possibilities of reducing the impact of increased unsprung mass. Besides, the addition of passive suspension components such as inerter [10] and relaxation spring [11] has proven to give significant improvements over the conventional suspension layout [12, 13]. The focus of this paper is to analytically derive the inerter and relaxation spring parameters to achieve performance benefits. Six suspension architectures having inerter and relaxation spring in different layouts are considered for the study. The dynamic performance of the suspension architectures is evaluated using three indices, namely, discomfort index, road holding index, and working space index. Starting from the analytical expressions of the performance indices, a comparison is made using a reference electric vehicle parameters. The analytical derivations of the performance indices provide an effective way to define the inerter equivalent mass and relaxation spring stiffness for improving the suspension dynamic behaviour.

The paper is organised as follows. Section 2 presents the six suspension architectures featuring inerter and relaxation springs along with the conventional suspension components. The analytical expressions of the performance indices are derived and presented. In Section 3, the suspension architectures are

compared analytically and the values of inerter equivalent mass and relaxation spring stiffness which improves the dynamic behaviours of in-wheel motor electric vehicle are derived.

2 System model

2.1 Quarter-car model and suspension architectures

The linear two-degree-of-freedom quarter-car model shown in Fig.1 includes the unsprung mass (m_1), the sprung mass (m_2), the tire radial stiffness (k_1), the external road excitation in the vertical direction (r), and the suspension strut. Even if the linear quarter-car model does not represent the full vehicle and does not include the non-linear properties of the suspension components, it contains the basic features of the real problem [14]. The assumption that the tyre is in contact with the ground is also not always true [15]. However, the quarter car model can effectively be used in the early design optimisation to obtain the preliminary results.

The conventional suspension strut S1, shown in Fig.2, has a parallel connected spring and damper. The other five suspension architectures with different arrangement of the inerter and/or relaxation spring are named as S2 to S6 [16]. The suspension spring stiffness, damping ratio, inerter equivalent mass, and relaxation spring stiffness are noted as k_2, r_2, m_e and k_3, respectively.

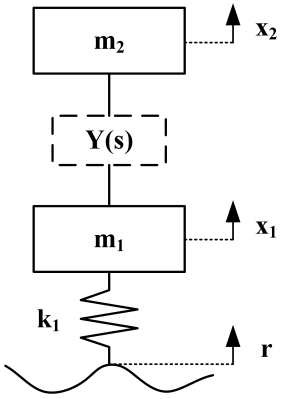

Figure 1: Quarter-car model

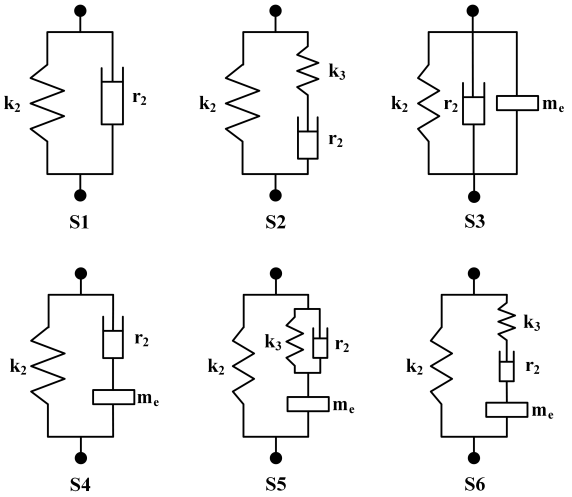

Figure 2: Suspension strut architectures

2.2 Analytical derivation of performance indices

The generic equations of motion of the quarter-car model can be written as

$$\begin{aligned} m_1 s^2 X_1 + k_1(X_1 - R) - sY(s)(X_2 - X_1) = 0 \\ m_2 s^2 X_2 + sY(s)(X_2 - X_1) = 0 \end{aligned} \tag{1}$$

The performance indices of suspension architectures can be modelled by substituting their mechanical admittance $Y(s)$ in (1). X_1 and X_2 are the Laplace forms of the vertical displacement of the unsprung mass (x_1) and the sprung mass (x_2) respectively. The parameter R represents the Laplace form of the vertical excitation due to the road irregularity r, which is defined by a single slope power spectral density (PSD) [6].

The vehicle body vertical acceleration ($\ddot{x}_2$), the dynamic tire load (F_z), and the relative displacement between wheel and vehicle body ($x_2 - x_1$) can be derived from the equations of motion (1). The variances of such quantities are considered as the performance indices which are named discomfort index ($\sigma^2_{\ddot{x}_2}$), road holding index ($\sigma^2_{F_z}$), and working space index ($\sigma^2_{x_2-x_1}$), respectively. The analytical expressions of the performance indices for all the architectures are presented in Appendix A.

3 Comparative analysis of suspension architectures

The performance of suspension architectures with inerter and/or relaxation spring are compared with that of the conventional suspension S1. The difference is evaluated by subtracting the corresponding performance indices, which are $\sigma^2_{\ddot{x}_2,Si} - \sigma^2_{\ddot{x}_2,S1}$ for discomfort index, $\sigma^2_{F_z,Si} - \sigma^2_{F_z,S1}$ for road holding index, and $\sigma^2_{x_2-x_1,Si} - \sigma^2_{x_2-x_1,S1}$ for working space index. Optimum values of the inerter equivalent mass (m_e) and relaxation spring stiffness (k_3) are defined as functions of the vehicle parameters (m_1, m_2, k_1, k_2, r_2). While comparing the suspensions architectures, the vehicle parameters are assumed to be fixed and the values of m_e and k_3 are varied to get improved performances. The parameters of a prototype electric vehicle driven by in-wheel motors are listed in Tab.1, together with the road roughness parameter (A_b) and vehicle velocity (v) [17]. The architecture S3 will not be analysed in detail, since the inerter in S3 does not provide any performance improvement over S1 as analysed in [12].

Table 1: Data of the reference electric vehicle [17] and driving condition.

Parameter	Unit	Value
m_1	kg	38
m_2	kg	202
k_1	N/m	200000
k_2	N/m	22366
r_2	N s/m	1627
A_b	m	1.4e-5
v	m/s	20

3.1 Comparison of S2 and S4 with S1

The architectures S2 and S4 have the inerter and relaxation spring in series with the damper respectively. The results show that the S2 improves road holding index, but worsens working space index. The difference in discomfort index is negligible. The architecture S4 improves the discomfort index, but the road holding index and working space index are worsened.

3.1.1 Difference in discomfort index

Based on the expressions of performance indices, the difference in discomfort index between the architecture S2 and S1 is derived as

$$\sigma^2_{\ddot{x}_2,S2} - \sigma^2_{\ddot{x}_2,S1} = \frac{A_b v k_1 k_2 r_2 (k_2 + 2k_3)}{2k_3^2 m_2^2} \tag{2}$$

It can be seen from (2) that the difference is greater than zero for any positive value of k_3, which means that the S1 is always better than S2 on discomfort index. For the reference vehicle parameters and the k_3 corresponding to the maximum benefit on road holding index, the discomfort index is 12% worse.

Similarly, the difference in discomfort index between the architecture S4 and S1 is derived as

$$\sigma^2_{\ddot{x}_2,S4} - \sigma^2_{\ddot{x}_2,S1} = \frac{A_b v k_2 r_2 \left(k_1 m_2^2 + k_2 (m_1 + m_2)^2 - 2k_1 m_e (m_1 + m_2)\right)}{2k_1 m_2^2 m_e^2}. \tag{3}$$

However, it is not straight forward to judge if the architecture S4 has better performance than S1 from (3). Therefore, the difference in discomfort index is presented as m_e varies in Fig.3(a) considering the parameters of the reference vehicle. It can be observed that S4 performs better than S1 on discomfort index when

$$m_e > \frac{k_1 m_2^2 + k_2 (m_1 + m_2)^2}{2k_1 (m_1 + m_2)} \tag{4}$$

There exist a value of m_e that corresponds to the largest difference between S1 and S4. By using this equivalent mass ($m^*_{e,minDC,S4}$ in the Fig.3(a)) for the inerter, the architecture S4 can achieve the maximum benefit on discomfort index (11%) .

$$m^*_{e,minDC,S4} = \frac{k_1 m_2^2 + k_2 (m_1 + m_2)^2}{k_1 (m_1 + m_2)} \tag{5}$$

3.1.2 Difference in road holding index

The difference in road holding index between the architecture S2 and S1 is derived as

$$\sigma^2_{F_z,S2} - \sigma^2_{F_z,S1} = \frac{A_b v k_1 r_2 \left(k_1 m_2 d_1 - k_1 k_3 m_2 d_2 + k_2^2 d_3^2 + 2 k_2 k_3 d_3^2\right)}{2 k_3^2 m_2^2}. \tag{6}$$

where

$$\begin{aligned} d_1 &= k_1 m_2 - 2 k_2 m_1 - k_2 m_2 \\ d_2 &= 2 m_1 + m_2 \\ d_3 &= m_1 + m_2 \end{aligned} \tag{7}$$

Further analysis indicates that the relaxation spring in S2 gives better road holding index than S1 when

$$k_3 > \frac{k_1 m_2 (k_1 m_2 - 2 k_2 m_1 - k_2 m_2) + k_2^2 (m_1 + m_2)^2}{k_1 m_2 (2 m_1 + m_2) - 2 k_2 (m_1 + m_2)^2}. \tag{8}$$

The difference in road holding index is plotted in Fig.3(b) and the maximum difference (9%) is observed at

$$k^*_{3,minRH,S2} = \frac{2\left(k_1 m_2 (k_1 m_2 - 2 k_2 m_1 - k_2 m_2) + k_2 (m_1 + m_2)^2\right)}{k_1 m_2 (m_2 - 2 m_1) - 2 k_2 (m_1 + m_2)^2} \tag{9}$$

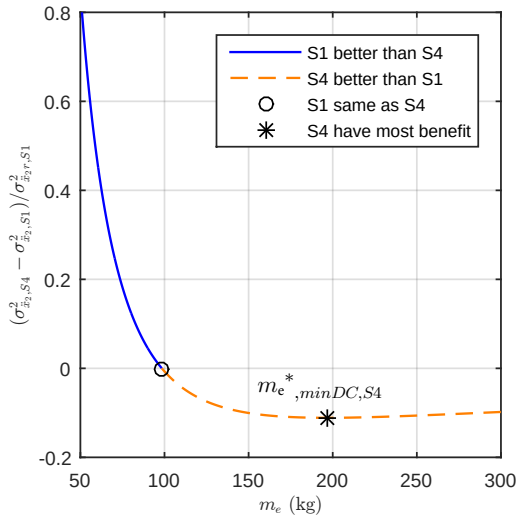

(a) Difference in discomfort index between S4 and S1

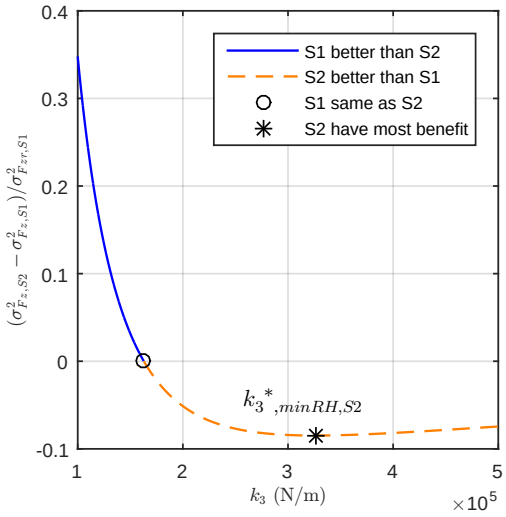

(b) Difference in road holding index between S2 and S1

Figure 3: Comparison of S2 and S4 with S1

The difference between S4 and S1 in road holding index is shown in (10).

$$\sigma^2_{F_z,S4} - \sigma^2_{F_z,S1} = \frac{A_b v r_2 \left(k_1^2 d_4 - k_1 k_2 d_5 - 2 k_1 k_2 m_e d_3^3 + k_2^2 d_3^4\right)}{2 k_1 m_2^2 m_e^2} \tag{10}$$

where

$$\begin{aligned} d_4 &= m_1 m_2 (m_1 m_2 + 2 m_1 m_e + 2 m_2 m_e) \\ d_5 &= 2 m_1^3 m_2 + 3 m_1^2 m_2^2 - m_2^4 \end{aligned}$$

The difference is always greater than zero for any positive value of m_e, which means the S4 is always worse than S1 on road holding index. For the reference vehicle and the m_e corresponding to the maximum benefit on discomfort index, the road index holding is 6% worse.

3.1.3 Difference in working space index

The difference between S2 and S1 in working space index is derived as shown in (11). The difference is always positive for any positive value of k_3, which means architecture S2 does not perform better than S1 on working space index (2% difference is observed considering the reference vehicle and k_3 value given in (9) that corresponds to the maximum benefit on road holding index).

$$\sigma^2_{x_2-x_1,S2} - \sigma^2_{x_2-x_1,S1} = \frac{A_b v k_1 r_2}{2k_3^2} \tag{11}$$

Similarly, the difference between S4 and S1 on working space index is shown in (12). The difference is positive for any positive value of m_e. The architecture S4 gives reduced performance on working space index over S1 (60% difference is observed considering the reference vehicle and m_e value given in (5) that corresponds to the maximum benefit of discomfort index).

$$\sigma^2_{x_2-x_1,S4} - \sigma^2_{x_2-x_1,S1} = \frac{A_b v r_2 \left(k_1 m_2^2 + k_2 (m_1+m_2)^2\right)}{2k_1 k_2 m_e^2} \tag{12}$$

3.2 Comparison of S5 and S6 with S1

The architectures S5 and S6 have both the inerter and relaxation spring arranged in different ways, as shown in Fig.2. Similar to the comparison made in Section 3.1, the architectures S5 and S6 are compared against S1 and the differences are derived analytically. But the analytical expressions are not given in the paper considering their complexity. It has been observed that the architecture S5 provides better performance in all the three performance indices compared to S1, while the S6 can improve only discomfort index and road holding index.

3.2.1 Difference in discomfort index

The difference in discomfort index considering the reference vehicle parameters is plotted in Fig.4. Same as the previous subsections, the region in blue represents the positive difference, which means S1 has better performance than S5 and S6. On the contrary, the region in orange gives the values of k_3 and m_e where S1 performs worse than S5 and S6.

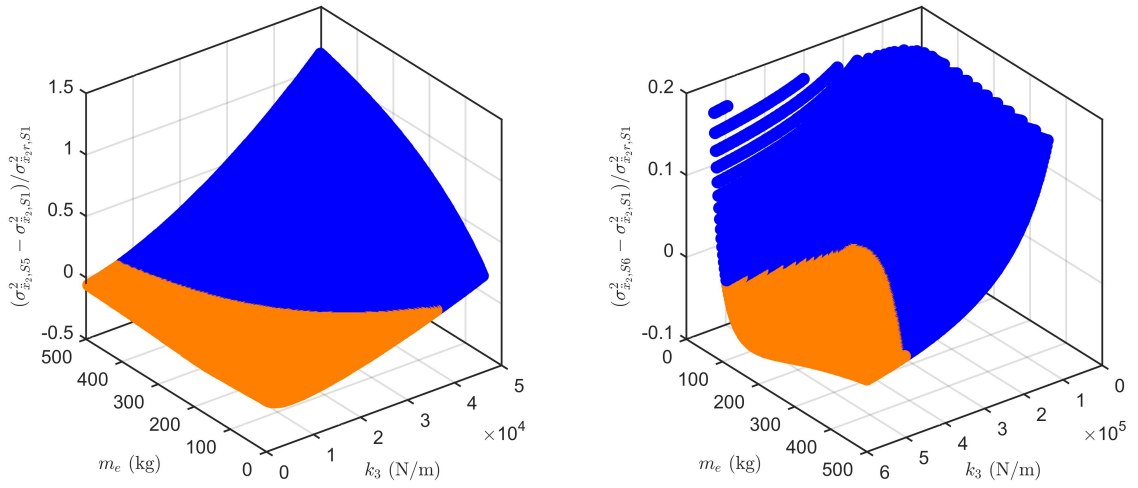

(a) Difference in discomfort index between S5 and S1

(b) Difference in discomfort index between S6 and S1

Figure 4: Difference in discomfort index

3.2.2 Difference in road holding index

Similarly, the difference in road holding index considering the reference vehicle parameters is plotted in Fig.5.

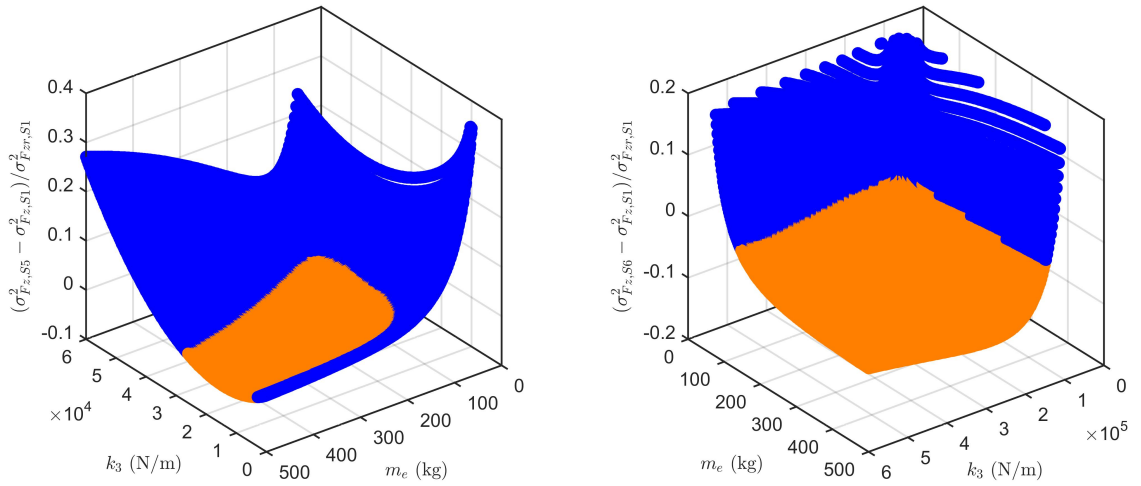

(a) Difference in road holding index between S5 and S1

(b) Difference in road holding index between S6 and S1

Figure 5: Difference in road holding index

3.2.3 Difference in working space index

Figure 6 shows the improvement on working space index provided by S5 as a function of m_e and k_3. The architecture S6 is not presented since it worsens the working space index.

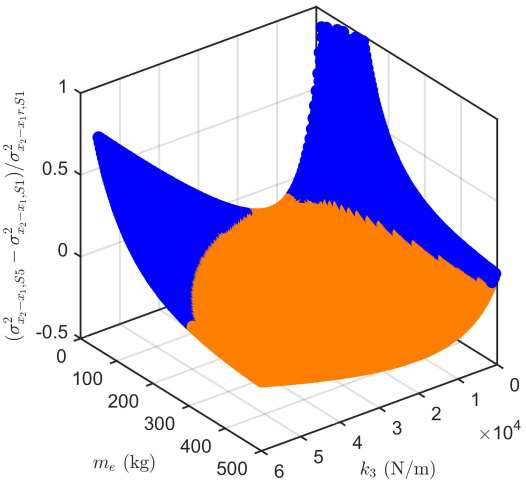

Figure 6: Difference in working space index between S5 and S1

4 Comparison of suspension architectures

The increased unsprung mass (m_1=38 kg) of IWM electric vehicle compared to the conventional vehicle (m_1=23 kg) deteriorates the suspension performance in all the three performance indices as in Tab. 2. Especially, the road holding index is worsened by 26.9%. The maximum possible benefits offered by the considered suspension architectures on road holding index is also presented here. Based on the results, one can understand that the possible benefits from inerter and relaxation spring are limited if the other design parameters are not varied. Hence, it is necessary to consider the k_2 and r_2 as design variables in the optimisation as in [12].

Table 2: Influence of inerter and relaxation spring on the suspension performance. The vehicle parameters and fixed values k_2 and r_2 are given in Tab. 1. The negative sign represents the improvement on performance index. The positive sign shows the deterioration on performance index.

	k_3 (N/m)	m_e (kg)	$\frac{\sigma^2_{\ddot{x}_2,Si}-\sigma^2_{\ddot{x}_2,S1}}{\sigma^2_{\ddot{x}_2,S1}}$	$\frac{\sigma^2_{F_z,Si}-\sigma^2_{F_z,S1}}{\sigma^2_{F_z,S1}}$	$\frac{\sigma^2_{x_2-x_1,Si}-\sigma^2_{x_2-x_1,S1}}{\sigma^2_{x_2-x_1,S1}}$
S1 without IWM	-	-	-1.2%	-26.9%	-6.3%
S1 with IWM	-	-	1	1	1
S2 with IWM	325785	-	11.6%	-8.5%	2.1%
S4 with IWM	-	197	-7.0%	+1.4%	+9.3%
S5 with IWM	21660	219	+7.3%	-3.3%	-32.1%
S6 with IWM	286693	428	+4.6%	-9.2%	+11.1%

5 Conclusions

For the electric vehicles driven by in-wheel motors (IWM), the weight of unsprung mass is higher than in conventional vehicles. In order to mitigate the drawbacks of increased unsprung mass, five suspension architectures with inerter and/or relaxation springs are taken into account to improve the dynamic behaviours of conventional spring-damper suspension. The performance indices, namely, discomfort index, road holding index, working space index of each suspension architectures are derived analytically and compared individually with the conventional suspension S1 of the vehicle having IWM. The differences in suspension performances are presented in detail. The architectures S2 and S4 can reduce the variance of dynamic tire load (8.5%) and the variance of vehicle body vertical acceleration (11%), respectively. The architecture S5 can improve the suspension dynamic behaviours in all the three performance indices (29% on discomfort index, 3% on road holding index, 33% on working space index). On the other hand, the S6 reduces the variance of vehicle body acceleration (6%) and dynamic tire load (9%), but increases the variance of working space marginally. However, the improvements offered by the inerter and relaxation spring are not sufficient to completely mitigate the problems associated with the increased unsprung mass in IWM electric vehicles. Further improvements on the performance are possible if the suspension spring and damper are changed.

References

[1] C., Espanet et. Al., *In-wheel motor for a small hybrid electric vehicle: design, realisation and experimental characterisation*, Energy Conversion Congress and Exposition (ECCE), 2012, 892-898.

[2] A. Watts, A. Vallance, A. Fraser et. Al., *Integrating in-wheel motors into vehicles-real-world experiences*, SAE International Journal of Alternative Powertrains, ISSN 2167-4205, 1(2012), 289-307.

[3] D. K. Perovic, *Making the impossible, possible-overcoming the design challenges of in wheel motors*, International Battery, Hybrid and Fuel Cell Electric Vehicle Symposium (EVS26), 5(2012), 514-519.

[4] A. M. El-Refaie, *Motors/generators for traction/propulsion applications: A review*, IEEE Vehicular Technology Magazine, ISSN 1556-6072, 8(2013), 90-99.

[5] A. Watts, A. Vallance et. Al., *The technology and economics of in-wheel motors*, SAE International Journal of Passenger Cars-Electronic and Electrical Systems, ISSN 1946-4622, 3(2010), 37-55.

[6] M. Gobbi, G. Mastinu, *Analytical description and optimization of the dynamic behaviour of passively suspended road vehicles*, Journal of Sound and Vibration, ISSN 1095-8568, 245(2001), 457-481.

[7] N. Borchardt, R. Kasper, W. Heinemann, *Design of a wheel-hub motor with air gap winding and simultaneous utilization of all magnetic poles*, Electric Vehicle Conference (IEVC), 2012, 1-7.

[8] Y. Luo, D. Tan, *Study on the dynamics of the in-wheel motor system*, IEEE Transactions on Vehicular Technology, ISSN 0018-9545, 61(2012), 3510-3518.

[9] R. Wang, H. Jing et. Al., *Optimization and finite-frequency H control of active suspensions in in-wheel motor driven electric ground vehicles*, Journal of the Franklin Institute, ISSN 0016-0032, 352(2015), 468-484.

[10] M. C. Smith, *Synthesis of mechanical networks: The inerter*, IEEE Transactions on Automatic Control, ISSN 0018-9286, 47(2002), 1648–1662.

[11] D. Ryba, *Improvements in dynamic characteristics of automobile suspension systems part 1. two-mass systems*, Vehicle System Dynamics, ISSN 0042-3114, 3(1974), 17-46.

[12] K. Ramakrishnan, L. Yang et. Al., *Multi-objective optimization of road vehicle passive suspensions with inerter*, ASME 2016 IDETC/CIE. American Society of Mechanical Engineers, 2016.

[13] M. C. Smith, F. C. Wang, *Performance benefits in passive vehicle suspensions employing inerters*, Vehicle System Dynamics, ISSN 0042-3114, 42(2004), 235-257.

[14] G. Mastinu, M.Ploechl, *Road and off-road vehicle system dynamics handbook*, ISBN 0-84933-322-9, CRC Press, 2014.

[15] R. N. Jazar, *Vehicle dynamics: theory and application*, ISBN 1-46148-543-6, New York, Springer, 2014.

[16] F. Scheibe, M. C. Smith, *Analytical solutions for optimal ride comfort and tyre grip for passive vehicle suspensions*, Vehicle System Dynamics, ISSN 0042-3114, 47(2009), 1229-1252.

[17] W. Tong, Z. Hou, *Vertical vibration analysis on electric vehicle with suspended in-wheel motor drives*, Electric Vehicle Symposium and Exhibition (EVS27), 2013.

Appendix A: Analytical expression of performance indices

The mechanical admittance of each suspension architectures and the detailed derivation of the standard deviations of $\ddot{x}_2$, F_z, and $x_2 - x_1$ can be found in [12]. In this paper, the variances of $\ddot{x}_2$, F_z, and $x_2 - x_1$ are considered as the objective functions. The analytical expressions of the discomfort index, road holding index, and working space index are given for all the architectures.

Discomfort index

The discomfort index $\sigma^2_{\ddot{x}_2,Si}$ is defined as the variance of the vehicle body vertical acceleration, which can be expressed as

$$\sigma^2_{\ddot{x}_2,Si} = A_b v \overline{\sigma}^2_{\ddot{x}_2,Si} \tag{13}$$

where the term $\overline{\sigma}^2_{\ddot{x}_2,Si}$ depends on the i-th suspension model in Fig.2.

For the suspension architecture S1,

$$\overline{\sigma}^2_{\ddot{x}_2,S1} = a_1 r_2 + a_2 r_2^{-1} \tag{14}$$

where

$$a_1 = \frac{k_1}{2m_2^2}; \quad a_2 = \frac{(m_1 + m_2)k_2^2}{2m_2^2}$$

For the suspension architecture S2,

$$\overline{\sigma}^2_{\ddot{x}_2,S2} = \sigma^2_{\ddot{x}_2,S1} + (a_3 k_3^{-1} + a_4 k_3^{-2}) r_2 \tag{15}$$

where

$$a_3 = \frac{k_1 k_2}{m_2^2}; \quad a_4 = \frac{k_1 k_2^2}{2m_2^2}$$

For the suspension architecture S3,

$$\overline{\sigma}^2_{\ddot{x}_2,S3} = a_1 r2 + \left(\frac{a_8 m_e^3 + a_7 m_e^2 + a_6 m_e + a_5}{a_{10} m_e + a_9} \right) r_2^{-1} \tag{16}$$

where

$$\begin{aligned} a_5 &= m_1 m_2 (m_1 + m_2) k_2^2 \\ a_6 &= (m_1 + m_2)^2 k_2^2 - 2 m_1 m_2 k_1 k_2 \\ a_7 &= -2 k_1 (m_1 + m_2) k_2 + m_2 k_1^2 \\ a_8 &= k_1^2 \\ a_9 &= 2 m_2^3 m_1 \\ a_{10} &= 2 (m_1 + m_2) m_2^2 \end{aligned}$$

For the suspension architecture S4,

$$\overline{\sigma}^2_{\ddot{x}_2,S4} = (a_1 + a_{11} m_e^{-1} + a_{12} m_e^{-2}) r_2 + a_2 r_2^{-1} \tag{17}$$

where

$$a_{11} = -\frac{(m_1 + m_2) k_2}{m_2^2}; \quad a_{12} = \frac{(m_1 + m_2)^2 k_2^2 + k_1 m_2^2 k_2}{2 m_2^2 k_1}$$

For the suspension architecture S5,

$$\begin{aligned} \overline{\sigma}^2_{\ddot{x}_2,S5} &= \overline{\sigma}^2_{\ddot{x}_2,S1} + (a_{11} m_e^{-1} + a_{12} m_e^{-2}) r_2 \\ &\quad + \left((a_{13} + a_{14} m_e^{-1} + a_{15} m_e^{-2}) k_3^2 - (a_{11} + 2 a_{12} m_e^{-1}) k_3 \right) r_2^{-1} \end{aligned} \tag{18}$$

where

$$\begin{aligned} a_{13} &= \frac{(m_1 + m_2)}{m_2^2} \\ a_{14} &= -\frac{2(m_1 + m_2)^2 k_2 + m_2^2 k_1}{2 m_2^2 k_1} \\ a_{15} &= \frac{(m_1 + m_2)^3 k_2^2 + 2 m_2^2 (m_1 + m_2) k_1 k_2 + m_2^3 k_1^2}{2 (m_2 k_1)^2} \end{aligned}$$

For the suspension architecture S6,

$$\overline{\sigma}^2_{\ddot{x}_2,S6} = \overline{\sigma}^2_{\ddot{x}_2,S2} + (a_{11} m_e^{-1} + a_{12} m_e^{-2} - 2 a_2 m_e^{-1} k_3^{-1}) r_2 \tag{19}$$

Road holding index

The road holding index $\sigma^2_{F_z,Si}$ is defined as the variance of dynamic tire load, which can be expressed as

$$\sigma^2_{F_z,Si} = A_b v \overline{\sigma}^2_{F_z,Si} \tag{20}$$

where the term $\overline{\sigma}^2_{F_z,Si}$ depends on the i-th suspension model in Fig.2.

For the suspension architecture S1,

$$\overline{\sigma}^2_{F_z,S1} = b_1 r_2 + b_2 r_2^{-1} \tag{21}$$

where

$$\begin{aligned} b_1 &= \frac{(m_1 + m_2)^2 k_1}{2 m_2^2} \\ b_2 &= \frac{(m_1 + m_2)^3 k_2^2 - 2 m_1 m_2 (m_1 + m_2) k_1 k_2 + m_1 (m_2 k_1)^2}{2 m_2^2} \end{aligned}$$

For the suspension architecture S2,

$$\overline{\sigma}^2_{F_z,S2} = \sigma^2_{F_z,S1} + (b_3 k_3^{-1} + b_4 k_3^{-2}) r_2 \tag{22}$$

where

$$\begin{aligned} b_3 &= \frac{2(m_1+m_2)^2 k_1 k_2 - m_2(m_2+2m_1)k_1^2}{2m_2^2} \\ b_4 &= \frac{(m_1+m_2)^2 k_1 k_2^2 - m_2(m_2+2m_1)k_1^2 k_2 + m_2^2 k_1^3}{2m_2^2} \end{aligned}$$

For the suspension architecture S3,

$$\overline{\sigma}^2_{F_z,S3} = b_1 r_2 + (b_2 - b_3 m_e + b_5 m_e^2) r_2^- 1 \tag{23}$$

where

$$b_5 = \frac{(m_1+m_2)k_1^2}{2m_2^2}$$

For the suspension architecture S4,

$$\overline{\sigma}^2_{F_z,S4} = (b_1 + b_6 m_e^{-1} + b_7 m_e^{-2}) r_2 + b_2 r_2^{-1} \tag{24}$$

where

$$\begin{aligned} b_6 &= \frac{-(m_1+m_2)^3 k_2 + m_1 m_2 (m_1+m_2) k_1}{m_2^2} \\ b_7 &= \frac{(m_1+m_2)^4 k_2^2 + (m_1+m_2)^2 (m_2-2m_1) m_2 k_1 k_2 + (m_1 m_2 k_1)^2}{2m_2^2 k_1} \end{aligned}$$

For the suspension architecture S5,

$$\overline{\sigma}^2_{F_z,S5} = \overline{\sigma}^2_{F_z,S1} + (b_6 m_e^{-1} + b_7 m_e^{-2}) r_2 + ((b_8 + b_9 m_e^{-1} + b_{10} m_e^{-2}) k_3^2 - (b_6 + 2b_7 m_e^{-1}) k_3) r_2^{-1} \tag{25}$$

where

$$\begin{aligned} b_8 &= \frac{(m_1+m_2)^3}{2m_2^2} \\ b_9 &= \frac{-(m_1+m_2)^4 k_2 + m_2(m_1+m_2)^2(2m_1-m_2)k_1}{2m_2^2 k_1} \\ b_{10} &= \frac{m_1+m_2}{2m_2^2 k_1^2}((m_1+m_2)^4 k_2 + 2m_2(m_1+m_2)^2(m_2-m_1)k_1 k_2 \\ &\quad + (m_1^2 - m_1 m_2 + m_2^2)(m_2 k_1)^2) \end{aligned}$$

For the suspension architecture S6,

$$\overline{\sigma}^2_{F_z,S6} = \overline{\sigma}^2_{F_z,S2} + (b_6 m_e^{-1} + b_7 m_e^{-2} - 2b_2 m_e^{-1} k_3^{-1}) r_2 \tag{26}$$

Working space index

The working space index $\sigma^2_{x_2-x_1,Si}$ is defined as the variance of the relative displacement between wheel and vehicle body, which can be expressed as

$$\sigma^2_{x_2-x_1,Si} = A_b v \overline{\sigma}^2_{x_2-x_1,Si} \tag{27}$$

where the term $\overline{\sigma}^2_{x_2-x_1,Si}$ depends on the i-th suspension model in Fig.2.

For the suspension architecture S1,

$$\overline{\sigma}^2_{x_2-x_1,S1} = c_1 r_2^{-1} \tag{28}$$

where For the suspension architecture S2,

$$\overline{\sigma}^2_{x_2-x_1,S2} = \sigma^2_{x_2-x_1,S1} + c_2 k_3^{-2} r_2 \tag{29}$$

where

$$c_1 = \frac{m_1+m_2}{2}; c_2 = \frac{k_1}{2}$$

For the suspension architecture S3,

$$\overline{\sigma}^2_{x_2-x_1,S3} = (m_1+m_2)/(2r_2) \tag{30}$$

For the suspension architecture S4,

$$\overline{\sigma}^2_{x_2-x_1,S4} = c_3 m_e^{-2} r_2 + c_2 r_2^{-1} \tag{31}$$

where

$$c_3 = \frac{(m_1+m_2)^2}{2k_1} + \frac{m_2^2}{2k_2}$$

For the suspension architecture S5,

$$\overline{\sigma}^2_{x_2-x_1,S5} = \frac{N1}{2D} + \frac{N2}{D} \tag{32}$$

where

$$\begin{aligned}
D =& r_2(-k_1k_2^2k_3^2D_1 + k_3(k_1^3k_2m_2^2m_e^4 + m_e^3D_2 + m_e^2D_3) + k_1^3k_2^2m_2^2m_e^4)\\
D_1 =& (m_1+m_2)^3m_e^3 + 3m_1m_2(m_1+m_2)^2m_e^2 + 3m_1^2m_2^2(m_1+m_2)m_e + m_1^3m_2^3\\
D_2 =& k_1^2k_2^2m_2^2(m_1+m_2) - k_1k_2^3(m_1+m_2)^3 + 2k_1^3k_2m_2^3\\
D_3 =& k_1^3k_2m_2^4 + k_1^2k_2^2m_2^3(m_1+3m_2) + k_1k_2^3m_2(-m_1^3 + m_1^2m_2 + 5m_1m_2^2 + 3m_2^3)\\
&+ k_2^4(m_1+m_2)^4\\
N_1 =& k_1^3k_2^2m_2^2m_e^2N_{11} + k_1^3k_2m_2^2m_e^2N_{12} + k_1k_2^2k_3^2m_2^2m_e^2N_{13} + k_1^2k_2k_3m_2^2r_2^2N_{14}\\
&+ k_1^2k_2^2m_2^2m_e^2N_{15}\\
N_{11} =& m_2m_e^2 + m_2^2m_e + m_2^3 + m_1m_e^2\\
N_{12} =& k_3m_2m_e^2 - k_3m_2^2m_e + m_2^2r_2^2 + k_3m_1m_e^2 + k_3m_1m_2^2\\
N_{13} =& (m_1+m_2)^3\\
N_{14} =& m_1m_2^2 + m_2^2m_e^2 + m_1^2m_e^2\\
N_{15} =& -k_3m_2^2m_e + m_2^2r_2^2 - k_3m_1^2m_e + k_3m_1^2m_2 + m_1^2r_2^2 + k_3m_1m_2^2\\
N_2 =& k_1^3k_2k_3m_1m_2^2m_e^3 + k_1^2k_2k_3m_2^2m_eN_{21} + k_1^2k_2^2m_1m_2^3m_e^2N_{22}\\
N_{21} =& k_3m_2(m_2^2m_e - 2m_1^2m_e - m_1m_2m_e) - k_3m_1^2m_2^2 - k_3m_e^2(m_1+m_2)^2\\
&+ m_1m_2r_2^2(m_1+m_2+m_e)\\
N_{22} =& r_2^2 - k_3m_e
\end{aligned}$$

For the suspension architecture S6,

$$\overline{\sigma}^2_{x_2-x_1,S6} = \overline{\sigma}^2_{x_2-x_1,S2} + (c_7 m_e^{-2} - 2c_2 m_e^{-1}k_3^{-1})r_2 \tag{33}$$

Authors

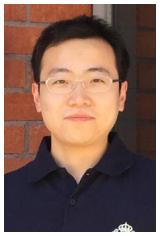

Liunan Yang was born in Xi'an, China. He received his Master degree in Engineering Design at KTH Royal Institute of Technology, Sweden. He is currently a Ph.D. student at Politecnico di Milano, funded by Chinese Scholarship Council. His research interests are the Multi-objective optimisation of complex mechanical systems, especially on the vehicle chassis subsystems.

Kesavan Ramakrishnan was born in Tamilnadu, India. He received Master degree in Automotive engineering from Clemson University, USA, in 2013. Currently he is a Marie-Curie research scholar in Politecnico di Milano, Italy. His research interests are electric vehicle powertrain modelling and controls, analytical modelling of PM machines, and Multi-objective optimisation of complex systems.

Federico Ballo received Master and doctoral degrees in Mechanical Engineering from Politecnico di Milano in 2011 and 2015 respectively. From 2015 up today he is working as research fellow at Politecnico di Milano. His main research fields are Multi-objective optimisation applied to the design of vehicle systems and components, structural optimisation, tyre modelling, and fatigue of vehicle wheels.

Giorgio Previati received Master and doctoral degrees in Mechanical Engineering from Politecnico di Milano in 2002 and 2006 respectively. From 2006 to 2008, he was employed at the Research and Development Centre of the SAME-Deutz-Fahr Group. Since December 2008, he became a researcher at Politecnico di Milano. Previati mainly concerns the study of complex systems with particular reference to land vehicles and their subsystems.

Massimiliano Gobbi is an Professor of Mechanical Engineering at Politecnico di Milano. He received Master and doctoral degrees in Applied Mechanics from Politecnico di Milano, Italy, in 1994 and 1998 respectively. His areas of interest are road vehicles engineering, optimisation of complex systems, advanced design, experimental mechanics. He is chair of the Vehicle Design Committee (VDC) of the ASME.

Gianpiero Mastinu was born in Sardinia, Italy. He received Master and doctoral degrees in Applied Mechanics from Politecnico di Milano, Italy, in 1984 and 1989 respectively. He was appointed as a Full Professor at TU Delft in 2000 and later at Politecnico di Milano in 2004. His scientific activities are focused on design, construction, and testing of machines, structures, and mechanical systems with particular reference to ground vehicles.